Chaos, Solitons and Fractals 171 (2023) 113480

Contents lists available at ScienceDirect

Chaos, Solitons and Fractals

journal homepage: www.elsevier.com/locate/chaos

# Plastic neural network with transmission delays promotes equivalence between function and structure

Paulo Ricardo Protachevicz [a,b,*], Fernando da Silva Borges [c,d], Antonio Marcos Batista [e,f], Murilo da Silva Baptista [b], Iberê Luiz Caldas [a], Elbert Einstein Nehrer Macau [g], Ewandson Luiz Lameu [h]

[a] Physics Institute, University of São Paulo, São Paulo, SP, Brazil
[b] Institute for Complex Systems and Mathematical Biology, SUPA, University of Aberdeen, Aberdeen, United Kingdom
[c] Department of Physiology and Pharmacology, State University of New York Downstate Health Sciences University, Brooklyn, NY, USA
[d] Center of Mathematics, Computation and Cognition, Federal University of ABC, São Bernardo do Campo, SP, Brazil
[e] State University of Ponta Grossa, Ponta Grossa, PR, Brazil
[f] Mathematics and Statistics Department, State University of Ponta Grossa, Ponta Grossa, PR, Brazil
[g] Federal University of São Paulo, São José dos Campos, SP, Brazil
[h] Cell Biology and Anatomy Department, Hotchkiss Brain Institute, University of Calgary, Calgary, Alberta, Canada

ARTICLE INFO

*Keywords:*
Synaptic plasticity
Hodgkin–Huxley model
Neural dynamics
Synchronisation

ABSTRACT

The brain is formed by cortical regions that are associated with different cognitive functions. Neurons within the same region are more likely to connect than neurons in distinct regions, making the brain network to have characteristics of a network of subnetworks. The values of synaptic delays between neurons of different subnetworks are greater than those of the same subnetworks. This difference in communication time between neurons has consequences on the firing patterns observed in the brain, which is directly related to changes in neural connectivity, known as synaptic plasticity. In this work, we build a plastic network of Hodgkin–Huxley neurons in which the connectivity modifications follow a spike-time dependent rule. We define an internal-delay among neurons communicating within the same subnetwork, an external-delay for neurons belonging to distinct subnetworks, and study how these communicating delays affect the entire network dynamics. We observe that the neuronal network exhibits a specific connectivity configuration for each synchronised pattern. Our results show how synaptic delays and plasticity work together to promote the formation of structural coupling among the neuronal subnetworks. We conclude that plastic neuronal networks are able to promote equivalence between function and structure meaning that topology emerges from behaviour and behaviour emerges from topology, creating a complex dynamical process where topology adapts to conform with the plastic rules and firing patterns reflect the changes on the synaptic weights.

## 1. Introduction

Signal transmission delays are an intrinsic property of neuronal communication and are extremely relevant in brain activities [1,2]. Asl et al. highlighted the importance of realistic time delays, emphasising that this property has just been marginally taking into account the used models over the decades [3]. The synaptic conduction delay is proportional to the axonal distance from the soma [4] and the experimental conduction velocity is 300 μm/ms in rat [5]. Therefore, neurons that are closer together have lower latencies, while communication between neurons in different hemispheres of the brain may have delays of a few hundred milliseconds [6]. Lameu et al. [7] showed that small values of the synaptic delay are related to synchronisation while non-trivial topology is presented in networks with high delay. However, in some cases, the synaptic delay can be associated with synchronisation suppression [8,9]. Different transmission or synaptic delays can generate synchronous and asynchronous neuronal activities [10,11].

Maps of neuronal circuits obtained from functional magnetic resonance imaging (fMRI) show the existence of modules in brain networks [12]. Sporns and Betzel [13] discussed how this modular formation may be related to brain evolution favouring the emergence of functional specialisation and complex dynamics. Lin et al. [14] observed the fMRI and electrophysiological timing information delays during a visuomotor reaction-time task across five brain regions. Latency matrices of 9321 brain subregions from fMRI signals showed structures

* Corresponding author at: Institute for Complex Systems and Mathematical Biology, SUPA, University of Aberdeen, Aberdeen, United Kingdom.
*E-mail address:* protachevicz@gmail.com (P.R. Protachevicz).

https://doi.org/10.1016/j.chaos.2023.113480
Received 31 January 2023; Received in revised form 31 March 2023; Accepted 17 April 2023

associated with different sensory states and brain functions [15]. Sun et al. demonstrated that certain intra and inter-networks delays can facilitate fast regular firings [16]. Know and Choe [17] pointed to a possible role of facilitation dynamics to compensate such delays in motor neurons by a systematic approach.

Synaptic plasticity is the fundamental ability of the neurons to change their connection intensities due to spike activities [18]. It has been reported that memory and learning functions are supported by synaptic plasticity in the brain [19]. Experimental data suggest that synchronous spike dynamics patterns can be intensified due to the plasticity, being associated with long-term memory processing. However, it is not completely clear how plasticity and synchronisation are related [20]. Synaptic plasticity occurs by updating the connection strength depending on the difference of spiking times between pre and postsynaptic neurons. This function bounds topology with spiking time intervals and therefore with synchronisation. Different from networks that have fixed coupling, where synchronous behaviour emerges from topology, in the plastic network, topology emerges from behaviour and behaviour emerges from topology. This mutual influence creates a complex dynamical process where topology adapts to conform with the plastic rules and firing patterns reflect the changes on the synaptic weights that is not completely understood.

Kim and Lim [21] studied spike synchronisation in the presence of excitatory spike time-dependent plasticity (STDP). They observed a Matthew effect in synaptic plasticity due to a positive feedback mechanism. In a similar framework, they also study the effect of inhibitory STDP for the same network topology showing that both depression and potentiation of inhibitory connections can occur [22]. Studying the cerebellar ring network with synaptic plasticity, they still found that phase, anti-phase, and complex out-of-phase activities are involved in the long-term depression [23]. Soltoggio and Stanley [24] reported the relationship between local Hebbian plasticity and learning using a computational approach focused on the noise and weight saturation.

Aoki [25] demonstrated the self-organisation phenomena in a recurrent network of oscillators in the presence of synaptic plasticity identifying phase, anti-phase, coherent and chaotic activities. Phase, anti-phase and phase-lock activities are the main types of synchronisation observed between brain regions [26–29]. Klimesch et al. [30] reported the importance of phase synchronisation in various cognitive processes. Phase synchronisation has been observed in distant cortical areas with long conduction delays [31]. Some works also showed that time delay, synaptic types and connection densities play an important role in anti-phase synchronisation [32,33].

In this work, we study how the emergence of synchronised symmetric patterns between the subnetworks depends on the absence and presence of long-term plasticity and on internal and external transmission delays. The anatomy of neurons is directly related to the values of internal and external delays between subnetworks. The transmission velocity of the signal depends on the morphology of the dendrites and axons [34,35] and the cell processing time [36]. Moreover, the time required for neurons to communicate may be significantly extended due to the physical distance between the sending and receiving cells [37]. Neurons in the same subnetwork have propagation delays associated with dendritic trees, with values ranging from submilliseconds to a few milliseconds [38,39]. In connections between different subnetworks, the axonal propagation delay contributes greatly to signal latency [40]. Considering that internal delays among neurons inside a subnetwork are smaller than the external ones between subnetworks, we find that distinct patterns of synchronisation can be achieved by changing the delays. In the presence of plasticity, one of main motivations is to investigate how the connections between the subnetworks evolve from initially random to a more structured configuration. In this context, we are able to identify the stronger connections between the subnetworks related to specific synchronised patterns.

The increase of internal delays reduces the synchronous patterns inside the subnetworks. External delays, on the contrary, can promote collective synchronisation. Subnetworks in one group symmetry whose neurons are connected with small external delays are less synchronous than those neurons connected via large delays. In addition to that, the synchronisation in one group is higher than for two, three, and four group symmetry. In particular, we note that different types of neuronal synchronisation are related to the network structure between the subnetworks. Our results also suggest that synchronous behaviour reveals the structure being created due to the plasticity. More specifically, functional communities and their connections inferred by measurements of neural phase synchronisation reflect the subnetworks and their linkage structure provided by the structural topology of the synapses.

The paper is organised as follows: In Section 2, we introduce our plastic neuronal network of coupled HH neurons and the diagnostic tool to identify synchronisation. In Section 3, we present the results of our study about the effects of synaptic delays between neuronal subnetworks. In the last section, we draw our conclusions.

## 2. Plastic neuronal network

### 2.1. Hodgkin–Huxley model

We consider the type-II neuron model proposed by [41]. The individual dynamics of each Hodgkin–Huxley (HH) neuron in the network is given by

$$\begin{aligned} C\dot{V}_i &= I_i - g_{\mathrm{K}} n_i^4 (V_i - E_{\mathrm{K}}) \\ &\quad - g_{\mathrm{Na}} m_i^3 h_i (V_i - E_{\mathrm{Na}}) - g_L (V_i - E_{\mathrm{L}}) \\ &\quad + (V_{\mathrm{r}}^+ - V_i) \sum_{j=1}^{N} g_{ij} f_j (t - \tau_{ij}), \end{aligned} \tag{1}$$

$$\dot{n}_i = \alpha_{n_i}(v_i)(1 - n_i) - \beta_{n_i}(v_i) n_i, \tag{2}$$

$$\dot{m}_i = \alpha_{m_i}(v_i)(1 - m_i) - \beta_{m_i}(v_i) m_i, \tag{3}$$

$$\dot{h}_i = \alpha_{h_i}(v_i)(1 - h_i) - \beta_{h_i}(v_i) h_i, \tag{4}$$

$$\dot{f}_i = \frac{-f_i}{\tau_{\mathrm{s}}}. \tag{5}$$

Eq. (1) represents the membrane dynamics of the neuron $i$. $C$ ($\mu$F/cm$^2$) is the membrane capacitance and $I_i$ ($\mu$A/cm$^2$) is a constant current density chosen in the interval $[10, 11]$. Depending on the $I_i$ value, the HH model can exhibit silence, bistability, and repetitive spike firings [42–45]. Once one understands well how bifurcations and dynamical behaviour happens as a parameter is changed in a nonlinear dynamical system, it is natural to take that parameter as the one to induce heterogeneity in a network. Following this idea, we have considered the heterogeneity in the constant current in the regime of repetitive spike firings as done in the Refs. [7,46–48]. The parameters $g_{\mathrm{K}}$, $g_{\mathrm{Na}}$, and $g_{\mathrm{L}}$ are the conductance of the potassium, sodium, and leak ion channels, respectively. $E_{\mathrm{K}}, E_{\mathrm{Na}}$, and $E_{\mathrm{L}}$ are the reversal potentials for these ion channels. $V_{\mathrm{r}}^+$ corresponds to the excitatory reversal potential. $g_{ij}$ is the excitatory coupling strength from the presynaptic neuron $j$ to the postsynaptic neuron $i$ with maximum and minimum value within the interval $[0.0, 0.01]$. We consider that the neuron has no self-connections, implying $g_{ii} = 0$. $f_i(t)$ is the normalised synaptic current from the neuron $j$ to $i$. The state variable $f_i$ decays exponentially and it is updated to the unity ($f_i \to 1$) at the spike time $t_i$ of the neuron $i$ [49,50]. Eq. (5) corresponds to an exponential decay on the evolution of $f_i(t)$. The parameter $\tau_{\mathrm{s}}$ is the synaptic time decay and $\tau_{ij}$ the delay on the synaptic transmission [51–53]. The intensity of synaptic current with time delay on the signal transmission depends on the state of the pre and postsynaptic neuron. $\tau_{ij}$ assumes values $\tau_{\mathrm{int}}$ and $\tau_{\mathrm{ext}}$ for internal and external connections between the subnetworks, respectively. In Eqs. (2) and (3), the functions $m(v_i)$ and $n(v_i)$ represent the sodium and potassium activation, respectively. In Eq. (4), $h(v_i)$ is the function for sodium inactivation. The functions $\alpha_n$, $\beta_n$, $\alpha_m$, $\beta_m$, $\alpha_h$, and $\beta_n$ are given by

$$\alpha_n(v) = \frac{0.01v + 0.55}{1 - \exp(-0.1v - 5.5)}, \tag{6}$$

$$\beta_n(v) = 0.125\exp\left(\frac{-v-65}{80}\right), \quad (7)$$

$$\alpha_m(v) = \frac{0.1v+4}{1-\exp(-0.1v-4)}, \quad (8)$$

$$\beta_m(v) = 4\exp\left(\frac{-v-65}{18}\right), \quad (9)$$

$$\alpha_h(v) = 0.07\exp\left(\frac{-v-65}{20}\right), \quad (10)$$

$$\beta_h(v) = \frac{1}{1+\exp(-0.1v-3.5)}, \quad (11)$$

where $v = V/[\text{mV}]$. In our simulations, we consider $C = 1$ μF/cm$^2$, $E_{\text{Na}} = 50$ mV, $E_{\text{K}} = -77$ mV, $E_{\text{L}} = -54.4$ mV, $g_{\text{Na}} = 120$ mS/cm$^2$, $g_{\text{K}} = 36$ mS/cm$^2$, $g_{\text{L}} = 0.3$ mS/cm$^2$, and $\tau_s = 2.728$ ms. The reversal potential for excitatory connections is $V_r^+ = 20$ mV [54]. For the numerical integration, we use the Runge–Kutta fourth-order method with a time step equal to $\delta t = 0.01$ ms.

### 2.2. Spike-time dependent plasticity

Spike-time dependent plasticity (STDP) is a process that produces changes in the synaptic strength. It is calculated taking into consideration the times between the spikes of the postsynaptic neuron $t_i$ and the presynaptic neuron $t_j$. For each synaptic connection, the presynaptic neuron is that one which sends the signal while the postsynaptic neuron receives such signal. The intensity of the excitatory synaptic weight is defined by the coupling strength. The change in the excitatory synaptic weights $\Delta g_{ij}$ due to the time difference $\Delta t_{ij} = t_i - t_j$ is given by [46,55–57]

$$\Delta g_{ij} = \begin{cases} A_1 e^{(-\Delta t_{ij}/\tau_1)} & , \text{ if } \Delta t_{ij} \geq 0 \\ -A_2 e^{(\Delta t_{ij}/\tau_2)} & , \text{ if } \Delta t_{ij} < 0 \end{cases} \quad (12)$$

where $A_1 = 1$, $A_2 = 0.5$, $\tau_1 = 1.8$ ms, and $\tau_2 = 6$ ms. The synaptic weights are updated according to Eq. (12), where $g_{ij} \to g_{ij} + G \cdot \Delta g_{ij}$. The change rate of the synaptic weight is considered as $G = 10^{-5}$ mS/cm$^2$. The initial value of all excitatory synaptic weights is given by $g_{ij} = 0.001$ mS/cm$^2$. The minimal and maximal excitatory synaptic weight are considered in the interval $[g_{\min}, g_{\max}] = [0,0.1]$ nS.

Fig. 1 displays the plasticity curves described by Eq. (12) (red line) as a function of $\Delta t_{ij}$. This figure shows that the difference on the spike times in which plastic rule generates synaptic depression or synaptic potentiation. High values of the time difference generate synaptic changes close to zero, as shown in the figure. To exemplify such update protocol, suppose that there is a synaptic connection from the neuron $i$ to neuron $j$, as shown in the inset of Fig. 1. Neurons $i$ and $j$ are represented by the circles while the synaptic connection from neuron $i$ to neuron $j$ is represented by the arrow. If neuron $j$ spikes before the neuron $i$, $\Delta t_{ij}$ will be negative, and the change in the synaptic connection from neuron $i$ to neuron $j$ ($\Delta g_{ij}$) will be negative (for small $|\Delta t_{ij}|$) or zero (for large $|\Delta t_{ij}|$). In other way, considering the same synaptic connection from neuron $i$ to neuron $j$, but with neuron $i$ spiking before that neuron $j$, $\Delta t_{ij}$ will be positive, and the change in the synaptic connection ($\Delta g_{ij}$) will be positive (for small $|\Delta t_{ij}|$) or zero (for large $|\Delta t_{ij}|$).

### 2.3. A network of subnetworks

We consider $N = 400$ non-identical HH neurons separated into $S = 4$ subnetworks with $N_{\text{sub}} = 100$ neurons each one ($N = S \cdot N_{\text{sub}}$). The heterogeneity in the system is given by the neuron currents $I_i$. To facilitate the visualisation and interpretation of our results, we sorted neurons in each subnetwork in ascending order according to their spiking frequency (or $I$). Therefore, the neuron $i = 1$ has the slowest spiking frequency and the neuron $i = 100$ has the highest one. The neurons are connected by means of excitatory synapses. For the initial coupling configuration, each subnetwork has an internal all-to-all topology without self-connections (autapses) [58]. The connections between subnetworks or external ones are randomly distributed with a certain probability. Thus, the internal and external probability of connections are given by $p_{\text{int}} = 1$ and $p_{\text{ext}} = 0.05$, respectively [59,60]. New connections are not allowed between subnetworks, however, changes in the weights of initial external connections are permitted. The network does not evolve to a configuration of only one community due to the plasticity due to the fixed internal connection probability between the subnetwork. With regard to the subnetworks, we consider an internal and external transmission delay given by $\tau_{\text{int}}$ and $\tau_{\text{ext}}$, respectively.

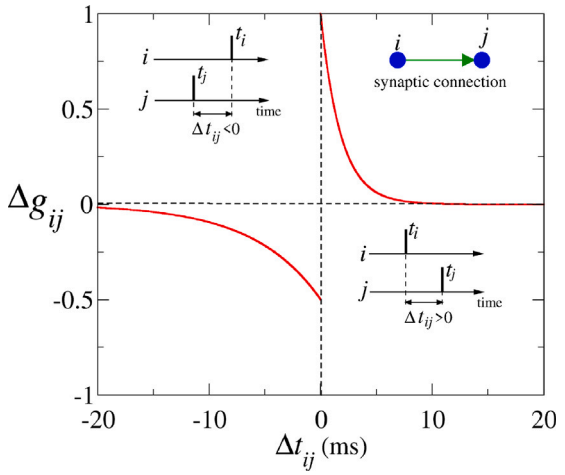


**Fig. 1.** Plasticity curves as a function of $\Delta t_{ij}$ for excitatory synapses. Negative and positive plus zero values of $\Delta t_{ij}$ correspond to synaptic depression and potentiation, respectively. The inset shows a schematic representation of the calculation of time difference $\Delta t_{ij}$ for a connection from neuron $i$ to neuron $j$, for the case of synaptic depression ($\Delta t_{ij} < 0$) and synaptic potentiation ($\Delta t_{ij} \geq 0$).

### 2.4. Measuring synchronisation and symmetries

In order to study neuronal synchronisation and symmetries, we compute the order parameter. Firstly, we use the traditional Kuramoto order parameter as a diagnostic tool for the whole network, that is given by [61]

$$R_{\text{T}}(t) = \left| \frac{1}{N} \sum_{j=1}^{N} e^{\text{i}\phi_j(t)} \right|, \quad (13)$$

where "i" is the imaginary unit $\sqrt{-1}$ and $\phi_j(t)$ is the neural phase associated with the spikes of each neuron $j$, given by

$$\phi_j(t) = 2\pi \frac{t - t_{j,k}}{t_{j,k+1} - t_{j,k}}, \quad (14)$$

$t_{j,k}$ is the time when a $k$-th spike ($k = 1, 2, 3, \dots$) happens in the neuron $j$ ($t_{j,k} < t < t_{j,k+1}$).

The time-average order parameter for the network is given by

$$\bar{R} = \frac{1}{t_{\text{fin}} - t_{\text{ini}}} \sum_{t_{\text{ini}}}^{t_{\text{fin}}} R_{\text{T}}(t), \quad (15)$$

in which $t_{\text{fin}} - t_{\text{ini}}$ is the time window set to measure the phases, where $t_{\text{ini}}$ and $t_{\text{fin}}$ correspond to the initial and final time of the analyses, respectively. In our simulations, we consider $t_{\text{ini}} = 80$ s and $t_{\text{fin}} = 100$ s. The magnitude of the time-average order parameter tends to the unity when the network has a globally synchronised behaviour. For uncorrelated spiking phases, the order parameter is close to 0.

The traditional Kuramoto order parameter for each subnetwork, $s = 1, 2, 3$, and 4, is described as

$$R_s(t) = \left| \frac{1}{N_{\text{sub}}} \sum_{j=(s-1)\cdot N_{\text{sub}}+1}^{s \cdot N_{\text{sub}}} e^{\text{i}\phi_j(t)} \right|. \quad (16)$$

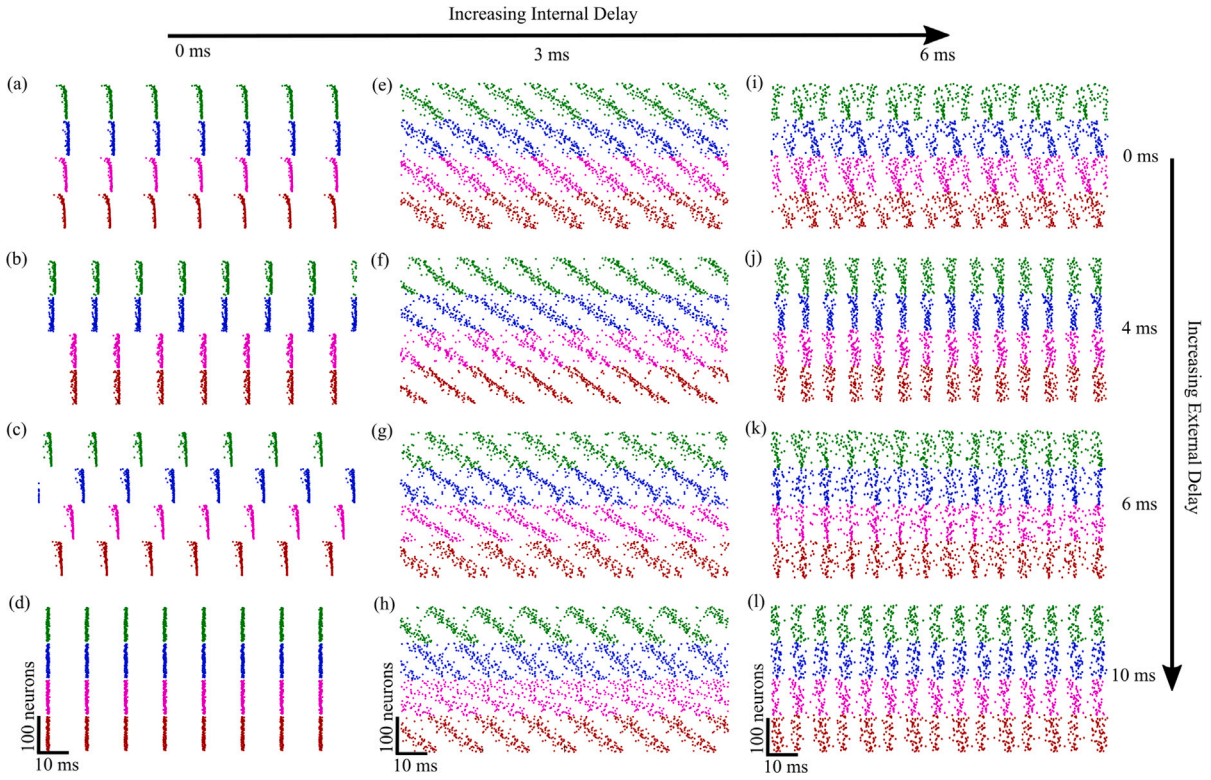


**Fig. 2.** Raster plots of all neurons $i$ for fixed internal ($\tau_{int}$) and external ($\tau_{ext}$) time delays when synaptic plasticity is active. Different colours denote each subnetwork. Figures (a–d), (e–h), and (i–l) display the raster plots for the internal time delays equal to $\tau_{int} = 0$ ms, $\tau_{int} = 3$ ms, and $\tau_{int} = 6$ ms, respectively. Figures (a,e,i), (b,f,j), (c,g,k), (d,h,l) display the raster plots for external time delays equal to $\tau_{ext} = 0$ ms, $\tau_{ext} = 4$ ms, $\tau_{ext} = 6$, ms and $\tau_{ext} = 10$ ms, respectively. For small internal delays, high synchronous patterns are observed in each subnetwork, while bigger internal ones generate less synchronised patterns. (For interpretation of the references to colour in this figure legend, the reader is referred to the web version of this article.)

In order to quantify and distinguish the different symmetric synchronisation patterns, we calculate the so-called $m$-th moment of the order parameter $R^m$ ($m$ is an index), that is a variation of Eq. (13) with $m = 1, 2, \ldots, S$ [62–64]

$$R^m = \left| \frac{1}{N} \sum_{j=1}^{N} e^{im\phi_j(t)} \right|. \tag{17}$$

The summation in Eq. (17) considers the phases of all neurons in the network. This measure allows us to quantify the number of synchronised neuronal groups and consequently the symmetry of their phase distributions. The calculation of the $m$-th moment is similar to the traditional order parameter with the difference that considers $m = 1$, 2, 3, or 4, multiplying each neuron phase. For the particular case where $m$=1, Eq. (17) is the same as Eq. (13). For the network composed of $S = 4$ subnetworks, we calculate all the moments $m \in [1, 4]$. The moment $R^m$ with the highest intensity (closer to 1) provides information about how the subnetworks are synchronised among them. They can vary from one big synchronised group to two or four groups, showing a fix phase difference among them. In this framework, the highest moment of order parameter gives us the information about synchronisation and type of symmetry configuration. For instance, if $R^1$ ($m = 1$) has the highest value (close to 1), the subnetworks have neurons forming effectively a single large network (small phase difference between subnetworks). If $R^2$ ($m = 2$) is the highest value, the neurons in subnetworks are synchronised in 2 groups in an anti-phase pattern (phase difference of $\pi$). The same idea applies for $m = 3$ and $m = 4$, where there are 3 and 4 groups, and the neurons in the groups have approximately $2\pi/3$ and $\pi/2$ phase differences, respectively. Table 1 exhibits the standard range of parameters that we consider in our simulations.

**Table 1**
Descriptions of the standard parameters and range values considered in our simulations.

| Descriptions | Parameter | Value |
|---|---|---|
| Number of subnetworks | $S$ | 4 |
| Neurons per subnetwork | $N_{sub}$ | 100 |
| Internal connect. probab. | $p_{int}$ | 1.0 |
| External connect. probab. | $p_{ext}$ | 0.05 |
| Internal time delay | $\tau_{int}$ | [0, 6] ms |
| External time delay | $\tau_{ext}$ | [0, 12] ms |
| Exc. synaptic conductance | $g_{exc}$ | [0, 0.01] mS/cm$^2$ |
| Membrane capacity | $C$ | 1.0 μF/cm$^2$ |
| Potassium conductance | $g_K$ | 36 mS/cm$^2$ |
| Sodium conductance | $g_{Na}$ | 120 mS/cm$^2$ |
| Leak conductance | $g_l$ | 0.3 mS/cm$^2$ |
| Potassium rev. potential | $V_K$ | −77 mV |
| Sodium reversal potential | $V_{Na}$ | 50 mV |
| Leak reversal potential | $V_l$ | −54.4 mV |
| Excitatory reversal potential | $V_r^+$ | 20 mV |
| Constant current | $I_i$ | [10,11] μA/cm$^2$ |
| Change rate of synap. weight | $G$ | $10^{-5}$ mS/cm$^2$. |
| Time step integration | $\delta t$ | $10^{-2}$ ms |
| Initial time for analyses | $t_{ini}$ | 80 s |
| Final time for analyses | $t_{fin}$ | 100 s |
| Internal time delay | $d_{int}$ | [0,1] ms |
| External time delay | $d_{ext}$ | [0,12] ms |
| Time step integration | $\delta t$ | $10^{-2}$ ms |

## 3. Results and discussions

In this work, we consider internal ($\tau_{int}$) and external ($\tau_{ext}$) delays in the subnetworks with and without the presence of STDP. Without plasticity, for small $\tau_{int}$ and varying $\tau_{ext}$, we observe different patterns

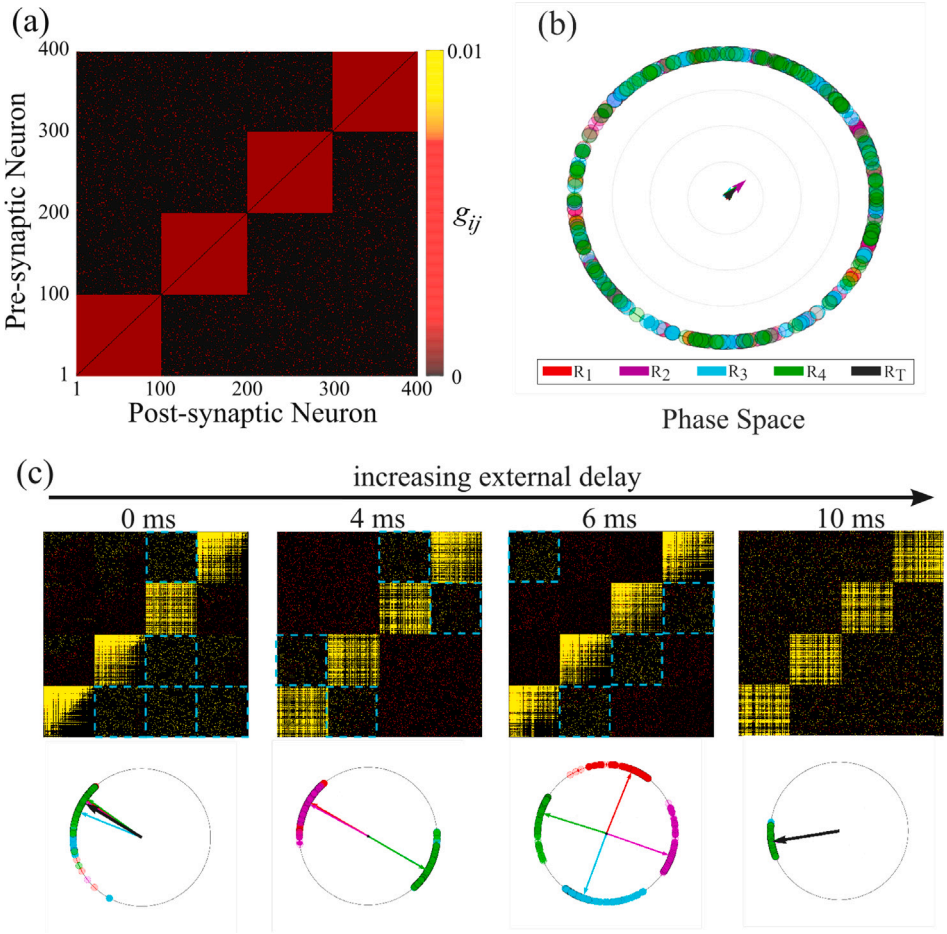


**Fig. 3.** The panel (a) displays the initial matrix configuration for all simulations, where the red colour represents the initial intensity of non null synaptic connections. Black indicates no synapses and yellow approximates to the maximal synaptic conductance $g_{ij}^{\max}$=0.01 mS/cm$^2$. The panel (b) shows the initial phases of all neurons in the network. The top panel in (c) exhibits the resultant matrix for fixed internal and external time delays. In bottom in panel (c), the traditional Kuramoto order parameter for the entire network is represented by a black arrow ($R_T(t)$), as well as the same order parameter considering each subnetwork is denoted by the red, violet, cyan, and green arrows ($R_s$). (For interpretation of the references to colour in this figure legend, the reader is referred to the web version of this article.)

of synchronisation between the subnetworks. However, our main goal is to investigate how these patterns of synchronisation affect the weights of network connections when plasticity is active. To do this, we consider different delay values which modify the dynamics of the network. We restricted the network to only excitatory neurons since the presence of inhibition in the current simulation generates very similar results.

Fig. 2 shows the raster plots for fixed internal and external time delays ($\tau_{\text{int}}$ and $\tau_{\text{ext}}$) when the synaptic plasticity is on. In the left side, we consider $\tau_{\text{int}}$ = 0 ms, (a) $\tau_{\text{ext}}$ = 0 ms, (b) $\tau_{\text{ext}}$ = 4 ms, (c) $\tau_{\text{ext}}$ = 6 ms, and (d) $\tau_{\text{ext}}$ = 10 ms. For small internal time delays, we verify synchronised symmetric patterns. In the centre column, we consider $\tau_{\text{int}}$ = 3 ms, (e) $\tau_{\text{ext}}$ = 0 ms, (f) $\tau_{\text{ext}}$ = 4 ms, (g) $\tau_{\text{ext}}$ = 6 ms, and (h) $\tau_{\text{ext}}$ = 10 ms. For these parameters, we observe no firing coherence, but the fastest neurons (higher $I_i$) in each subnetwork start firing and subsequently the slower neuron. In the right side, we use $\tau_{\text{int}}$ = 6 ms, (i) $\tau_{\text{ext}}$ = 0 ms, (j) $\tau_{\text{ext}}$ = 4 ms, (k) $\tau_{\text{ext}}$ = 6 ms, and (l) $\tau_{\text{ext}}$ = 10 ms. Although some synchronisation can be noticed, it is lower than in the case for $\tau_{\text{int}}$ = 0 ms. For $\tau_{\text{int}}$ = 0 ms, we identify an equal pattern for the case with and without plasticity, as shown in Fig. 2(a–d).

We focus on the most synchronised symmetric patterns. In Fig. 2(a), neuron spikes in a single group (almost complete phase synchronisation) without delay between the subnetworks. Highest order parameter is the one with order $m$=1, indicating all neurons spiking nearly synchronously. Fig. 2(b) displays neurons spiking in two groups for an external time delay equal to $d_{\text{ext}}$ = 4 ms. Highest order parameter is the one with order $m$=2. In Fig. 2(c), the neurons spike in four groups for an external time delay equal to $d_{\text{ext}}$ = 6 ms. Highest order parameter is the one with order m=4. For a delay close to the average period between spikes ($\approx$ 14 ms) the network returns to a single group, as shown in Fig. 2(d). In this case, the neurons of all subnetworks exhibit a strong phase synchronisation. These patterns can also be obtained for different parameters when there is no plasticity.

Fig. 3(a) displays the initial matrix connections $g_{ij}$ of the subnetworks. In Fig. 3(b), we plot the initial neuronal phases where each colour represents a subnetwork. The coloured arrows are the initial order parameters showing that initially the neurons are not synchronised. Fig. 3(c) exhibits the final coupling matrix after the plasticity actuates by 100 s, considering different values of the external delays and fixed internal delay $\tau_{\text{int}}$ = 0 ms. For $\tau_{\text{ext}}$ = 0 ms, we see a strong coherent dynamics among the subnetworks, all organised in a single group. The resulting network presents some hierarchical organisation where the directed connections between some subnetworks were reinforced as highlighted by the dashed blue squares in Fig. 3(c) (first column). For $\tau_{\text{ext}}$ = 4 ms, the network effectively forms two pairs of subnetworks with neurons belonging to different subnetworks having a constant phase difference around $\pi$ radians (anti-phase synchronisation). In this case, connections between in-phase subnetworks are potentiated and depressed for the anti-phase ones. For $\tau_{\text{ext}}$ = 6 ms, the network effectively presents four groups where neurons within each pair of groups have a phase difference around $\pi/2$ radians and the network is set to a configuration of subnetworks being connected under a ring topology. Considering $\tau_{\text{ext}}$ = 10 ms, the network goes effectively to one

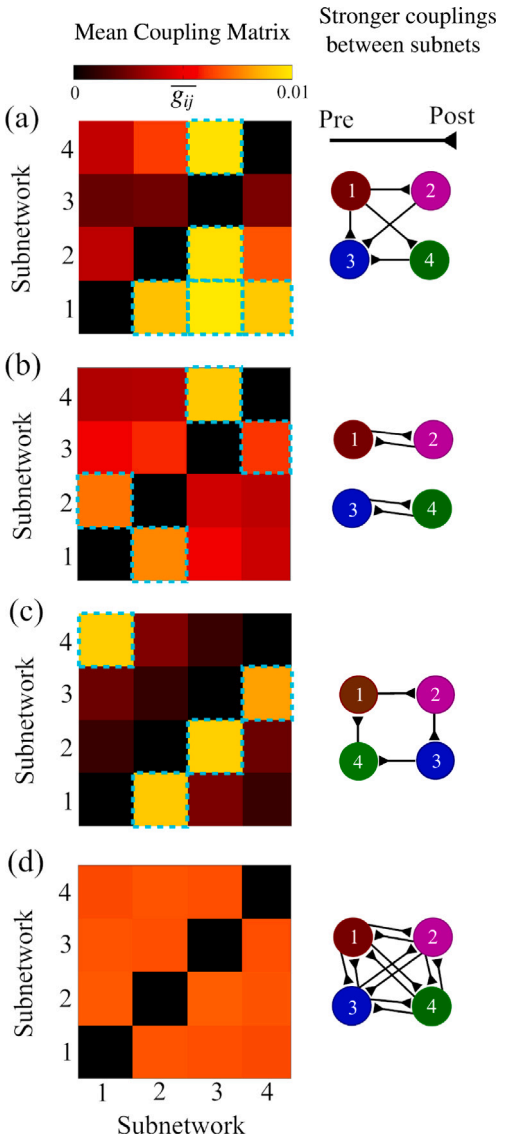


**Fig. 4.** Resultant mean synaptic weight (left) and schematic representation of resultant connections between the subnetworks (right) for $\tau_{int} = 0$ ms. The edges in the graphs plotted on the right column panel represent the presence of strong connections from one subnetwork to another. We consider (a) $\tau_{ext} = 0$ ms, (b) $\tau_{ext} = 4$ ms, (c) $\tau_{ext} = 6$ ms and (d) $\tau_{ext} = 10$ ms.

phase group formation, and the network topology shows no preferential connection among the subnetworks. Therefore, when the delay values come close to the time period of the spikes, the behaviour is similar to that observed when the connection delay between the subnetworks is close to zero and the synchronisation is improved. As the difference for one group synchronisation with small time delays, all connections between the subnetworks are potentiated.

In the synchronised regimes, the phase difference between groups is roughly constant, as seen in Fig. 3(c). The traditional Kuramoto order parameter is not capable to detect and classify all those synchronised configurations in addition to a single group. For this reason, we consider the $m$-th moments of the order parameter. The moments of the order parameter is a suitable diagnostic of symmetry between the synchronised subnetworks.

The left side of Fig. 4 shows the mean synaptic coupling between the subnetworks computed with the matrices from Fig. 3(c). The schematic representations of the stronger mean connection between the subnetworks are displayed on the right side. The strongest weight connections between the subnetworks can be associated to the average matrix, as highlighted by the blue dashed squares. The black line with a triangle at the end corresponds to the connection direction from a presynaptic subnetwork to a postsynaptic one. In Fig. 4(a), the strong phase synchronisation potentiates connections between the subnetworks in an asymmetric way. In this case, the neurons in the subnetwork 1 spike first, followed by subnetworks 2, 4, and 3. STDP is responsible for reshaping the network leading to the configurations depicted in Fig. 4(a), where the connection reinforcement follows the order of spikes. All connections from subnetwork 1 to 2, 3, and 4 are reinforced. The same happens with the connections from subnetwork 2 to 3 and 4, and from subnetwork 4 to 3. Fig. 4(b) exhibits two groups in anti-phase. The connections are reinforced between in-phase subnetworks and weakened between the two groups. In Fig. 4(c), the subnetworks show a phase-lock synchronisation with average phase difference of $\pi$ radians. These patterns lead to a ring network configuration. The connections are potentiated in a cyclic way. The subnetworks are in-phase synchronisation in Fig. 4(d) in a more coherent state than in Fig. 4(a). This strong synchronisation promotes an all-to-all connection organisation among subnetworks with an average reinforcement of the connections.

To better understand how plasticity promotes synchronised patterns, in Fig. 5, we calculate the $m$-th moments for $\tau_{int} = 0$ ms, (a) $\tau_{ext} = 0$ ms, (b) $\tau_{ext} = 4$ ms and (c) $\tau_{ext} = 6$ ms. To calculate the $R^m$, we consider the phase temporal evolution of all neurons of the network in Eq. (17), independent of their respective subnetwork, for each moment $m = 1$, 2, 3, and 4. We observe a higher 1-st moment in Fig. 5(a), which corresponds to a one-group phase synchronisation between the subnetworks. In this case, we verify that other moments are relatively lower than the first one. Fig. 5(b) displays a higher 2-nd moment due to an anti-phase synchronisation in two major groups. In Fig. 5(c), we identify a higher 4-th moment, which is associated with a phase-lock synchronisation between the subnetworks, as shown in Fig. 3(c). The higher moment of the order parameter indicates the symmetry of the synchronised patterns. It is worth to mention, that as can be seen in Figs. 3(a–c), the moments present a constant value overtime. Figs. 5 (d) and (e) exhibit the symmetric synchronised patterns in the parameter space $\tau_{ext} \times \tau_{int}$ without and with synaptic plasticity, respectively. In the case without plasticity and small external time delay, we find one group symmetry with phase synchronisation. Increasing the external delays, we identify predominantly 2 and 4 groups symmetry, respectively. For larger external delays (around 10 ms), the network returns to a one synchronised group. These cases are found for small internal time delays (less than 1 ms). For higher internal time delays (more than 1 ms), we observe less synchronised patterns. On the other hand, synaptic plasticity shifts to the left in $\tau_{ext}$, in which the regions where one, two, and four group symmetries are found. Moreover, the area in parameter space covering the existence of order 2 and 4 phase patterns is enlarged by plasticity. Then, not only plasticity allows for more complex patterns to emerge for smaller $\tau_{ext}$, but also the livelihood of its appearance for a large range of delays. Thus, plasticity promotes complexity as measured by the emergence of symmetric synchronous patterns. Figs. 5(f) and 5(g) show the higher values of the order parameters moments for the case without and with synaptic plasticity, respectively. We verify that the highest values of $R^m$ correspond to one group symmetry.

In summary, spiking synchronous patterns are strongly related to the network connection between subnetworks in a plastic neuronal network with time delay. For small external delays, one group configuration exhibits subnetworks spiking in a specific order, and this order promotes synaptic potentiation from the subnetworks spiking first to the subsequent ones. Increasing external delay, two group patterns generate potentiation in in-phase subnetworks, while a synaptic depression among the ones from distinct groups. For major delays, four groups (a phase-lock synchronisation between subnetworks) show a synchronised state, in which all subnetworks spiking almost at the same time and without any preferential order. This dynamical behaviour promotes

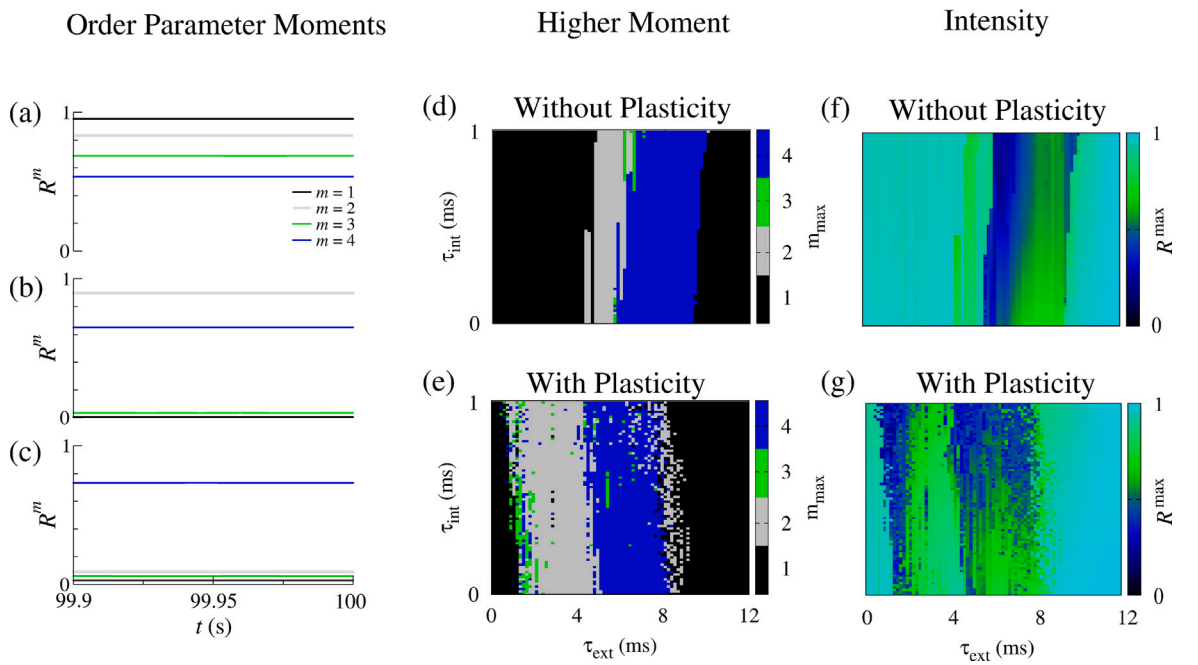


**Fig. 5.** The panels (a), (b), and (c) show the time evolution of the order parameter moments. We compute the time evolution of the order parameter moments for $\tau_{int} = 0$ ms, (a) $\tau_{ext} = 0$ ms, (b) $\tau_{ext} = 4$ ms, and (c) $\tau_{ext} = 6$ ms. The panels (d) and (e) display the symmetric patterns found in the parameter space of $\tau_{int}$ and $\tau_{ext}$ without and with plasticity, respectively. The panels (f) and (g) show the highest value of the order parameters moments in the space parameter of $\tau_{int}$ and $\tau_{ext}$ for the case without and with synaptic plasticity, respectively.

a final global network configuration with an average increase in all synaptic strengths. In all cases, the potentiation between the neuronal areas can also depend on the internal time delay. The less recurrent pattern found in our simulations is the 3 groups organisation, which can be associated with a transient behaviour.

## 4. Conclusions

In this work, we consider a network of subnetworks to study the effects of internal and external transmission delays on the generation of symmetric dynamics patterns, as well as the potentiation and depression on the synaptic weights due to the presence of plasticity. To do that, we consider Hodgkin–Huxley neurons coupled by means of excitatory chemical synapses and a time dependent plastic rule. To achieve synchronised patterns, the internal delayed transmission of neuron communication in the subnetworks assumes small values while the external one assumes higher values. When the internal transmission delay of neurons in the subnetworks assumes higher values, nonsynchronised patterns are observed.

Without plasticity and depending on the delay transmission between the subnetworks, we verify that synchronisation among subnetworks can be observed in different patterns. These regimes can be detected by means of the $m$-th moment of the order parameter, which provides the information about how the dynamics of neurons in the subnetworks are correlated in the phase space of spiking times. Due to the plasticity effect, we verify that the final connectivity reflects the symmetric synchronous patterns on the emergence of the strongest connections between the subnetworks. Thus, subnetworks that are strongly connected, are also strongly synchronous, and the same symmetric patterns observed in terms of synchronisation are also found in the final connecting topology. We show that the synaptic transmission delays play an important role in the generation of symmetric synchronised patterns. In addition, we also show that the phase, anti-phase, and symmetric phase-lock synchronised firing patterns influence the synaptic changes of the weight connections among the subnetworks. We observe the relationship of each symmetric synchronised firing pattern with the induced potentiation between the subnetworks. As a consequence, our results suggest that firing patterns can induce different topologies in addition to that topology induced firing patterns. We show that it is possible to identify spiking correlations with delayed excitatory connectivities between different neuronal groups.

A recent work [44] has proposed the construction of modular, scalable and adaptable neuronal networks with neurons possessing different dynamic properties and distinct firing patterns. To achieve that the authors considered neurons with different external input. In this work, we also consider heterogeneity in the external parameter. Our goal however was focused not on the design but on the relation between topology and synchronisation patterns. Whenever networks with STDP are designed with neurons that can have external currents controllable and accessible, our work shows that topology and synchronisation are strongly related.

Topology and behaviour is extensively studied in the literature. The novelty in our results was to study the emergency of different synchronous regimes, phase, anti-phase and shift phase. The emergency of these distinct regimes has been found in the brain. Experimental evidence shows that phase synchronisation is able to support memory processes and changes in the connection strengths [20,65]. In particular, results of Jutras and Buffalo suggest that phase synchronisation can lead to potentiation of the synaptic connections [66]. Our results can be linked to these experimental works, providing a possible explanation about how these synchronous firing patterns leads to a topology. Anti-phase oscillations are observed during rest state in humans [67] and in anaesthetised monkeys [68]. In addition, shift-phase synchronisation was observed in primary visual cortex [69] and could play a function to stimulus selection [70]. Our work shows that all these synchronous phenomena induce topology and emerge from it.

All these paving the way for us to conclude that plasticity – described by a pairwise function that regulates synapse strength by the time intervals between two spiking neurons – in fact promotes the creation of evolved network structures whose subnetworks of intra connected neurons and their inter connections is strongly reflected in the global synchronisation patterns measured by the phase dynamics of the neurons. Thus, the plastic neural network has a strong match between phase activity and graph structure.

## CRediT authorship contribution statement

**Paulo Ricardo Protachevicz:** Conceptualization, Data curation, Formal analysis, Investigation, Methodology, Validation, Visualization, Writing – original draft, Writing – review & editing. **Fernando da Silva Borges:** Conceptualization, Data curation, Formal analysis, Investigation, Methodology, Validation, Visualization, Writing – original draft, Writing – review & editing. **Antonio Marcos Batista:** Conceptualization, Supervision, Writing – original draft, Writing – review & editing. **Murilo da Silva Baptista:** Supervision, Writing – original draft, Writing – review & editing. **Iberê Luiz Caldas:** Supervision, Writing – original draft, Writing – review & editing. **Elbert Einstein Nehrer Macau:** Supervision, Writing – original draft, Writing – review & editing. **Ewandson Luiz Lameu:** Conceptualization, Data curation, Formal analysis, Investigation, Methodology, Validation, Visualization, Writing – original draft, Writing – review & editing.

## Declaration of competing interest

The authors declare that they have no known competing financial interests or personal relationships that could have appeared to influence the work reported in this paper.

## Data availability

Data will be made available on request.

## Acknowledgements

The authors acknowledge the financial support from São Paulo Research Foundation (FAPESP, Brazil) (Grants Nos. 2016/23398-8, 2017/13502-5, 2018/03211-6, 2020/04624-2, 2022/05153-9, 2022/13761-9), National Council for Scientific and Technological Development (CNPq), Fundação Araucária and Coordenação de Aperfeiçoamento de Pessoal de Nível Superior - Brasil (CAPES).

## References

[1] Petkoski S, Jirsa VK. Transmission time delays organize the brain network synchronization. Philos Trans R Soc A 2019;377:20180132.
[2] Sreenivasan KK, D'Esposito M. The what, where and how of delay activity. Nat Rev Neurosci 2019;20:466.
[3] Asl MM, Valizadeh A. Tass PA delay-induced multistability and loop formation in neuronal networks with spike-timing-dependent plasticity. Sci Rep 2018;8:12068.
[4] Borges FS, Moreira JVS, Takarabe LM, Lytton WW, Dura-Bernal S. Large-scale biophysically detailed model of somatosensory thalamocortical circuits in NetPyNE. Front Neuroinform 2022;16:884245.
[5] Stuart G, Schiller J, Sakmann B. Action potential initiation and propagation in rat neocortical pyramidal neurons. J Physiol 1997;505:617–32.
[6] Itoh K, Konoike N, Nejime M, Iwaoki H, Igahashi H, Hirata S, Nakamura K. Cerebral cortical processing time is elongated in human brain evolution. Sci Rep 2022;12:1103.
[7] Lameu EL, Macau EEN, Borges FS, Iarosz KC, Caldas IL, Borges RR, Protachevicz PR, Viana RL, Batista AM. Alterations in brain connectivity due to plasticity and synaptic delay. Eur Phys J 2018;227:673–82.
[8] Mugnaine M, Reis AS, Borges FS, Borges RR, Ferrari FAS, Iarosz KC, et al. Delayed feedback control of phase synchronisation in a neuronal network model. Eur Phys J Spec Top 2018;227:1151–60.
[9] Hansen M, Protachevicz PR, Iarosz KC, Caldas IL, Batista AM, Macau EEN. The effect of time delay for synchronization suppression in neuronal networks. Chaos Solit Fractals 2022;164:112690.
[10] Lubenov EV, Siapas AG. Decoupling through synchrony in neuronal circuits with propagation delays. Neuron 2008;58:118–31.
[11] Protachevicz PR, Borges FS, Iarosz KC, Baptista MS, Lameu EL, Hansen M, et al. Influence of delayed conductance on neuronal synchronization. Front Physiol 2020;11:1–9.
[12] Power JD, Cohen AL, Nelson SM, Wig GS, Barnes KA, Church JA, et al. Functional network organization of the human brain. Neuron 2011;72(4):665–78.
[13] Sporns O, Betzel RF. Modular brain networks. Annu Rev Psychol 2016;67:613–40.
[14] Lin F-H, Witzel T, Raij T, Ahveninen J, Tsai KW-K, Chu Y-H, et al. fMRI hemodynamics accurately reflects neuronal timing in the human brain measured by MEG. Neuroimage 2013;78:372–84.
[15] Guo B, Zhou F, Li M, Gore JC. Latency structure of BOLD signals within white matter in resting-state fMRI. Magn Res Imaging 2022;89:58–69.
[16] Sun X, Perc M, Kurths J, Lu Q. Fast regular firings induced by intra- and inter-time delays in two clustered neuronal networks. Chaos 2018;28:106310.
[17] Know J, Choe Y. Facilitating neural dynamics for delay compensation: A road to predictive neural dynamics? Neural Netw 2009;22:267–76.
[18] Ramirez A, Arbuckle MR. Synaptic plasticity: The role of learning and unlearning in addiction and beyond. Biol Psychiatry 2016;80:e73.
[19] Abraham WC, Jones OD, Glanzman DL. Is plasticity of synapses the mechanism of long-term memory storage? NPJ Sci Learn 2019;4:9.
[20] Fell J, Axamacher N. The role of phase synchronization in memory processes. Nat Rev Neurosci 2011;12:105.
[21] Kim S-Y, Lim W. Stochastic spike synchronization in a small-world neural network with spike-timing-dependent plasticity. Neural Netw 2018;97:92–106.
[22] Kim S-Y, Lim W. Effect of inhibitory spike-timing-dependent plasticity on fast sparsely synchronized rhythms in a small-world neuronal network. Neural Netw 2018;106:50–66.
[23] Kim S-Y, Lim W. Effect of diverse recoding of granule cells on optokinetic response in a cerebellar ring network with synaptic plasticity. Neural Netw 2021;134:173–204.
[24] Soltoggio A, Stanley KO. From modulated hebbian plasticity to simple behavior learning through noise and weight saturation. Neural Netw 2012;34:28–41.
[25] Aoki T. Self-organization of a recurrent network under ongoing synaptic plasticity. Neural Netw 2015;62:11–9.
[26] Tognoli E, Kelso JAS. Brain coordination dynamics: True and false faces of phase synchrony and metastability. Prog Neurobiol 2009;87:31.
[27] Thatcher RW. Coherence, phase differences, phase shift, and phase lock in EEG/ERP analyses. Dev Neuropsychol 2012;37:476–96.
[28] Carlos F-LP, Ubirakitan M-M, Rodrigues MCA, Aguilar-Domingo M, Herrera-Gutiérrez E, Gomez-Amor J, et al. Anticipated synchronization in human EEG data: Unidirectional causality with negative phase lag. Phys Rev E 2020;102:032216.
[29] Protachevicz PR, Hansen M, Iarosz KC, Caldas IL, Batista AM, Kurths J. Emergence of neuronal synchronization in coupled areas. Front Comput Neurosci 2021;15:1–12.
[30] Klimesch W, Freunberger R, Sauseng P, Gruber W. A short review of slow phase synchronization and memory: Evidence for control processes in different memory systems? Brain Res 2008;1235:31–44.
[31] Knoublauch A, Sommer FT. Spike-timing-dependent synaptic plasticity can form zero lag links for cortical oscillations. Neurocomputing 2004;52–54:301–6.
[32] Li D, Zhou C. Organization of anti-phase synchronization pattern in neural networks: What are the key factors?. Front Syst Neurosci 2011;5:1–14.
[33] Bodner M, Zhou YD, Shaw GL, Fuster JM. Symmetric temporal patterns in cortical spike trains during performance of a short-term memory task. Neurol Res 1997;19:509–14.
[34] Manor Y, Koch C, Segev I. Effect of geometrical irregularities on propagation delay in axonal trees. Biophys J 1991;60:1424–37.
[35] Boudkkazi S, Carlier E, Ankri N, Caillard O, Giraud P, Fronzaroli-Molinieres L, et al. Release-dependent variations in synaptic latency: A putative code for short-and long-term synaptic dynamics. Neuron 2007;56:1048–60.
[36] Wang HX, Gerkin RC, Nauen DW, Bi GQ. Coactivation and timing-dependent integration of synaptic potentiation and depression. Nature Neurosci 2005;8:187–93.
[37] Knoblauch A, Sommer FT. Synaptic plasticity, conduction delays, and inter-areal phase relations of spike activity in a model of reciprocally connected areas. Neurocomputing 2003;52:301–6.
[38] Agmon-Snir H, Segev I. Signal delay and input synchronization in passive dendritic structures. J Neurophysiol 1993;70:2066–85.
[39] Schierwagen A, Claus C. Dendritic morphology and signal delay in superior colliculus neurons. Neurocomputing 2001;38:343–50.
[40] Swadlow HA, Wey TG. Corticogeniculate neurons, corticotectal neurons, and suspected interneurons in visual cortex of awake rabbits: Receptive-field properties, axonal properties, and effects of eeg arousal. J Neurophysiol 1987;57:977–1001.
[41] Hodgkin AL, Huxley AF. A quantitative description of membrane current and its application to conduction and excitation in nerve. Physiol J 1952;11:500.
[42] Luccioli S, Kreuz T, Torcini A. Dynamical response of the Hodgkin–Huxley model in the high-input regime. Phys Rev E 2006;73:041902.
[43] Pospischil M, Toledo-Rodriguez M, Monier C, Piwkowska Z, Bal T, Frégnac Y, Markram H, Destexhe A. Minimal Hodgkin–Huxley type models for differents classes of cortical and thalamic neurons. Biol Cybernet 2008;99:427–41.
[44] Giannari AG, Astolfi A. Model design for networks of heterogeneous Hodgkin–Huxley neurons. Neurocomputing 2020;496:147–57.
[45] Shi Q, Han F, Wang Z, Li C. Rhythmic oscillations of excitatory bursting Hodgkin–Huxley neuronal network with synaptic learning. Comput Intell Neurosci 2016;6023547:1–9.
[46] Popovych OV, Yanchuk S, Tass PA. Self-organized noise resistance of oscillatory neural networks with spike timing-dependent plasticity. Sci Rep 2013;3:2926.
[47] Borges RR, Iarosz KC, Batista KC, Caldas IC, Borges FS, Lameu EL. Sincronização de disparos em redes neuronais com plasticidade sináptica. Rev Bras Ensino Fis 2015;37(2):2310.

[48] Borges RR, Borges FS, Lameu EL, Batista AM, Iarosz KC, Caldas IL, et al. Effect of the spike timing-dependent plasticity on the synchronization in a random Hodgkin–Huxley neuronal network. Commun Nonlinear Sci Numer Simulat 2016;34:12–22.
[49] Rothman JS, Silver RA. Data-driven modeling of synaptic transmission and integration. Prog Mol Biol Transl Sci 2014;123:305–50.
[50] Borges FS, Protachevicz PR, Lameu EL, Bonetti RC, Iarosz KC, Caldas IL, et al. Synchronised firing patterns in a random network of adaptive exponential integrate-and-fire neuron model. Neural Netw 2017;90:1–7.
[51] Asl MM, Valizadeh A, Tass PA. Dendritic and axonal propagation delays determine emergent structures of neuronal networks with plastic synapses. Sci Rep 2017;7:39682.
[52] Markram H, Lübke J, Frotscher M, Roth A, Sakmann B. Physiology and anatomy of synaptic connections between thick tufted pyramidal neurones in the developing rat neocortex. Physiol J 1997;500(2):409–40.
[53] Markram H, Lübke J, Frotscher M, Sakmann B. Regulation of synaptic efficacy by coincidence of postsynaptic APs and EPSPs. Science 1997;275:5297.
[54] Borges RR, Borges FS, Lameu EL, Batista AM, Iarosz KC, Caldas IL, et al. Spike timing-dependent plasticity induces non-trivial topology in the brain. Neural Netw 2017;88:58.
[55] Bi GQ, Poo MM. Synaptic modifications in cultured hippocampal neurons: Dependence on spike timing, synaptic strength, and postsynaptic cell type. J Neurosci Res 1998;18:10464.
[56] Markram H, Gerstner W, Sjöström PJ. Spike-timing-dependent plasticity: A comprehensive overview. Front Synaptic Neurosci 2012;4:2.
[57] Caporale N, Dan Y. Spike timing-dependent plasticity: A hebbian learning rule. Annu Rev Neurosci 2008;31:25–46.
[58] Protachevicz PR, Iarosz KC, Caldas IL, Antonopoulos CG, Batista AM, Kurths J. Influence of autapses on synchronization in neural networks with chemical synapses. Front Syst Neurosci 2020;14:604563.
[59] Schmidt M, Bakker R, Hilgetag CC, Diesmann M, van Albada SJ. Multi-scale account of the network structure of macaque visual cortex. Brain Struct Funct 2018;223:1409–35.
[60] Johnson RR, Burkhalter A. Microcircuitry of forward and feedback connections within rat visual cortex. J Comp Neurol 1996;368:383–98.
[61] Kuramoto Y. Chemical oscillations, waves, and turbulence. Berlin: Springer-Verlag; 1984.
[62] Sepulchre R, Paley DA, Leonard NE. Stabilization of planar collective motion: All-to-all communication. IEEE Trans Automat Control 2007;52:5.
[63] Lücken L, Yanchuk S, Popovych OV, Tass PA. Desynchronization boost by non-uniform coordinated reset stimulation in ensembles of pulse-coupled neurons. Front Comput Neurosci 2013;7:63.
[64] Jain A, Ghose D. Collective circular motion in synchronized and balanced formations with second-order rotational dynamics. Commun Nonlinear Sci Numer Simul 2018;54:156–73.
[65] Clouter A, Shapiro KL, Hanslmayr S. The phase synchronization is the glue that binds human associative memory. Curr Biol 2017;27:3143–8.
[66] Jutras MJ, Buffalo EA. Synchronous neural activity and memory formation. Curr Opin Neurobiol 2010;20(2):150–5.
[67] Fox MD, Raichle ME. Spontaneous fluctuations in brain activity observed with functional magnetic resonance imaging. Nat Rev Neurosci 2007;8:700.
[68] Vincent JL, Patel GH, Fox MD, Snyder AZ, Baker JT, Van Essen DC, et al. Intrinsic functional architecture in the anaesthetized monkey brain. Nature 2007;447:83–6.
[69] Vinck M, Lima B, Womelsdorf T, Oostenveld R, Singer W, Neuenschwander S, et al. Gamma-phase shifting in awake monkey visual cortex. J Neurosci 2010;30:1250–7.
[70] Tiesinga PH, Sejnowski TJ. Mechanisms for phase shifting in cortical networks and their role in communication though coherence. Front Hum Neurosci 2010;4.